

THERMAL PERFORMANCE ANALYSIS OF ELECTRIC VEHICLE CHARGING CONNECTORS

by

Xueyan LIN*

Beijing University of Posts and Telecommunications, Beijing, China

Original scientific paper
<https://doi.org/10.2298/TSCI200609313L>

In order to obtain the thermal characteristics of the electric vehicle connector in operation. Firstly, the thermal circuit diagram of the connector is obtained by using thermoelectric simulation method. Then, based on Newton's cooling equation, the natural-convection heat transfer coefficient of the connector is calculated, which provides accurate input parameters for thermal simulation calculation. Finally, the thermal performance of the connector and the influence of component size and material are analyzed based on ANSYS software. When the working current is 250 A and the ambient temperature is 25 °C, the temperature rise of connector shell and conductor can meet the thermal performance requirement. In order to reduce the temperature and uniform temperature difference of each part of the connector, the following optimization schemes are put forward: the optimal length of the insulator is 44 mm, the shell length should be increased as far as possible if conditions permit, and liquid crystal polymer with high thermal conductivity is selected as the insulator material, and aluminum alloy with high thermal conductivity and blackness is selected as the shell material.

Key words: *charging connector, natural convective heat transfer coefficient, ANSYS electrothermal simulation, heat performance, optimization*

Introduction

With the continuous development of electronic technology, semiconductor device circuit integration degree is higher and higher, the power of the module is larger and the physical size is smaller and smaller, and the heat flux density also increases. The formation of high heat flux density brings higher thermal control requirements for electronic components. Therefore, the effective solution the problem of heat dissipation has become the key technology to be solved urgently.

Garrett *et al.* [1] summarized several recent advances in vehicle thermal management technology and modelling, with a focus on three key areas: the cabin, electronics, and exterior components of vehicles. For thermal management of electronics, including batteries and insulated-gate bipolar transistors (IGBT), active and passive cooling methods that employed heat pipes, heat sinks, jet impingement, forced convection, and phase-change materials are discussed. Chen *et al.* [2] designed a thermal control system of electric cabinet in a high resolution space camera to resolve its heat dissipation. Several kinds of approaches in thermal conduction and thermal radiation were used to dissipate the heat for the electric components, printed circuit boards and their chassis. Based on the results of thermal test and thermal analy-

* Author's e-mail: xylin@bupt.edu.cn

sis, the thermal design was modified by adding a heat pipe. Liu *et al.* [3] prepared a new composite thermal interface material-AlN doped gallium based liquid metal silicone grease. The SEM and energy dispersive spectroscopy were used to detect the microstructure and chemical composition of the materials to study the thermal conductivity principle. The thermal conductivity could reach $5.014 \text{ [Wm}^{-1}\text{K}^{-1}\text{]}$. The experimental results show that the newly synthesized AlN doped gallium based liquid metal silicone grease can significantly reduce the operating temperature of notebook core, and have a wide application prospect. For a high-resolution space camera's shield, Jiang *et al.* [4] proposed several different thermal control schemes and carried out comparative analysis. The thermal design scheme with low power consumption and small temperature fluctuation range was selected. The effectiveness of the scheme was verified by heat balance test and on orbit data. According to the characteristics and mission requirements of star sensor on high-resolution satellite, Jiang *et al.* [5] carried out the thermal design of star sensor module by combining simulation analysis and experiment. The combination of passive thermal control and active thermal control is selected. The temperature range of the star sensor bracket was $17.0\sim 19.1 \text{ }^\circ\text{C}$ under low and high temperature conditions. The thermal balance test and on orbit temperature test verify that the thermal design is reasonable and effective and meets the mission requirements. The heat pipe with overall thickness less than 2 mm is called ultra-thin micro heat pipe, which was an effective means to solve the heat dissipation problem of light and thin electronic equipment in a narrow space. Tang *et al.* [6] introduced the type and applications of ultra-thin micro heat pipe, summarized the research progresses of wick structure and forming process of ultra-thin micro heat pipe, and discussed the problems existed on ultra-thin micro heat pipe technology.

In order to ensure that the temperature of electronic components does not exceed the allowable value, it is necessary to carry out thermal simulation analysis and thermal test. Su *et al.* [7] presented a method for thermal simulation of a plate fin heat sink using an analytical solution of the 3-D heat equation resulting from an appropriate plate fin heat sink transient thermal model. The entire solution methodology was illustrated in detail on the particular examples of the plate fin heat sink subjected non-uniform heat density on the surfaces. The transient temperature profiles were obtained for different positions at the surface of the plate fin heat sink. The analytical results were compared with measurements made on the surface of the cold plate and it was found that they were in good agreement with an error of less than 3 K. Wu *et al.* [8] established a 2-D mathematical model to analyze the thermal properties of thermal control unit (TCU) and calculated it numerically. The results showed that the design of ribbed and foamed phase change material composites could significantly improve the thermal performance of TCU and meet the requirements of electronic components well. To obtain the thermal performances of a motor controller working in stratosphere, Nie *et al.* [9] carried out thermal simulation analysis based on software ICEPAK, and verified the simulation model through ground environment simulation experiment and stratospheric flight experiment. The results showed that the thermal design of the controller can meet the requirements of heat preservation and dissipation. The internal fan could effectively keep the temperature balance of the controller under the condition of low stratospheric pressure. The solar radiation at stratosphere height had a great influence on the temperature distribution in the controller. Taking the IGBT water-cooled radiator for an electric vehicle converter as the research object, Ding *et al.* [10] used FLUENT software to calculate the steady-state results of IGBT water-cooled radiator. By using the self-developed model reduction calculation program, the transient problem of IGBT water-cooled radiator was quickly calculated, and the temperature curve of each chip of IGBT component at different time was obtained. The results showed that the heat dissipation perfor-

mance of the water-cooled radiator met the requirements of typical urban road conditions in China. Wang *et al.* [11] simulated the heat transfer of the hydraulic system of a 50 wheel loader, and compared the simulation results with the test data. The results showed that the accuracy of the simulation results can meet the engineering requirements, and the accuracy of the model could meet the needs of engineering design.

As consumers have more and more requirements for the internal electronic functions of the automobile, and the electronic functions that can be provided by the interior of the automobile are becoming more and more abundant, which makes the automotive connector one of the fastest growing market segments in the automotive parts. A typical light vehicle has about 1500 connectors, 50-60% of which are used for critical power distribution functions. The connectors of new energy vehicles are needed to withstand up to 250 A current and 600 V voltage. At the same time, they are used in increasingly harsh environment, including temperature (-40°C to 155°C), vibration, oxidation and friction Corrosion. When the larger working current flows through the connector, the connector will generate considerable Joule heat due to the effect of the body resistance and contact resistance of the contact. If the heat is not quickly transferred to the surrounding environment, it will inevitably bring a large temperature rise, as high as 200°C . Excessive temperature rise not only reduces the performance and reliability of the connector, but also leads to some vehicle failures and accidents. There is no condition for the connector to be fitted with an additional radiator, so it is necessary to analyze and design the natural air heat dissipation of the connector.

This paper takes an electric vehicle charging connector as the research object, and analyzes the thermal performance and influencing factors of the connector by simulation. Firstly, based on the law of energy conservation in thermodynamics, the thermal circuit of connector is analyzed by electrothermal simulation method, and the relationship between temperature rise, thermal resistance and current is deduced. Then, based on Newton's cooling equation, the dimensional analysis method and iterative method are used to calculate the convective heat transfer coefficient of the connector under natural air cooling, so as to provide accurate parameters for thermal simulation analysis. Finally, the thermal performance of the connector is simulated by ANSYS Workbench software, and the influence of connector size and material on temperature rise is analyzed, and the improvement scheme of connector heat dissipation performance is proposed.

Heat transfer analysis of electric vehicle charging connectors

Model and simplification

The research object is a charging connector of electric vehicles as shown in fig. 1. The connector is mainly composed of four parts: contact, insulator, shell, and accessories. The contact is the core part of the connector, and is obtained by matching the cylindrical pin of the plug with the crown spring socket. The thermal performance requirement of the connector is

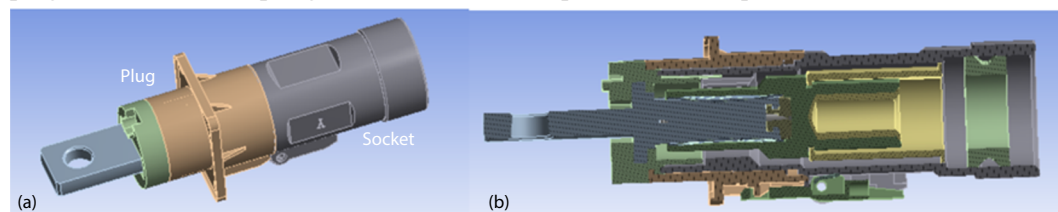


Figure 1. Structure of an electric vehicle charging connector; (a) outline drawing and (b) sectional drawing

that when the contact is connected with the rated working current of 250 A, the temperature rise between the connector shell and the environment does not exceed 45 °C.

Based on the complexity of the surface characteristics of the connector components, the actual charging connector is simplified and shown in fig. 2 for convenience of thermal analysis. The contact is simplified as a cylinder, and the insulator and shell are simplified as hollow cylinders with different radii. The dimensions and material parameters of the connector model are listed in tab. 1.

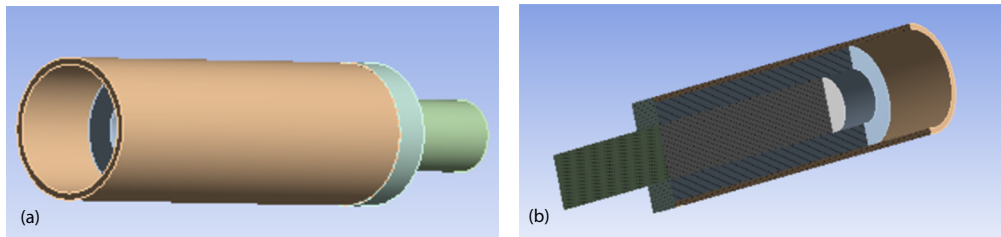


Figure 2. Simplified model of connector with insulator and shell; (a) exterior view and (b) sectional view

Table 1. Dimensions and material parameters of the connector model

	Internal diameter [mm]	External diameter [mm]	Length [mm]	Material	thermal conductivity, λ [$\text{Wm}^{-1}\text{C}^{-1}$]	Radiation coefficient, ϵ	Resistivity [Ωm]
Contact	10	–	61	Copper	330	0.01	$1.75 \cdot 10^{-8}$
Insulator	10	18	44	PA66	0.23	0.95	–
Shell	18	20	58	Aluminum alloy	104.7	0.2	–

Heat transfer of the connector

When current, I , flow through the contact conductor, Joule heat I^2R is generated due to the effect of the body resistance and contact resistance of the conductor, which makes the conductor temperature increases to T_c . In the connector, the heat is transferred to the shell through insulator with thermal resistance R_{i1} and shell with thermal resistance R_{i2} , so that the temperature of the shell is increased to T_w . The heat transferred to the shell is transferred to the external environment with temperature T_0 through the natural-convection heat transfer of the air with thermal resistance R_c , and through the radiation heat transfer with thermal resistance R_r .

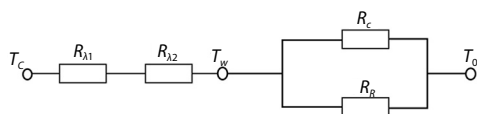


Figure 3. Heat transfer process (heat circuit diagram) of the charging connector

The thermal power, W_0 , generated by the connector:

$$W_0 = I^2 R = I^2 (R_b + R_j) = I^2 \left(\rho \frac{4l_d}{\pi d_d^2} + 0.89 \rho \sqrt{\frac{\zeta H}{nF}} \right) \quad (1)$$

where R_b is the body resistance of the contact conductor, R_j – the contact resistance produced when the cylinder pin and the crown spring socket are contacted, ρ , l_d , d_d , and H are the resistivity, length, diameter, and hardness of the contact conductor, respectively, ζ – the deformation coefficient of the contact pin and the crown spring socket, generally $\zeta = 0.7$, F – the contact

force between the pin and the crown spring socket. The thermal effect of the contact resistance is not considered in this paper, that is $R_j = 0$. Substituting the parameters in tab. 1 into eq. (1), it can be calculated that $R_b = 13.6 \mu\Omega$, when $I = 250 \text{ A}$, then $W_0 = 0.85 \text{ W}$.

The heat conduction power W_j and W_w of insulator and shell hollow cylinder can be obtained by Fourier heat conduction formula, as shown respectively:

$$W_j = \frac{2\pi\lambda_j l_j}{\ln \frac{d_{jw}}{d_{jn}}} (T_c - T_j) \quad (2)$$

$$W_w = \frac{2\pi\lambda_w l_w}{\ln \frac{d_{ww}}{d_{wn}}} (T_j - T_w) = \frac{2\pi\lambda_w l_w}{\ln \frac{d_{ww}}{d_{jw}}} (T_j - T_w) \quad (3)$$

where λ_j and λ_w are the thermal conductivity of insulator and shell material, respectively, l_j and l_w – the length of insulator and shell, respectively, d_{jw} and d_{jn} – the outer diameter and inner diameter of insulator, respectively, d_{ww} and d_{wn} – the outer diameter and inner diameter of shell, respectively, where $d_{jw} = d_{wn}$, and T_c , T_j , and T_w – the temperature of contact conductor, insulator and shell, respectively.

The thermal power, W_c , of convective heat transfer satisfies the Newtonian cooling equation as shown in eq. (4). The thermal power, W_r , of radiation heat transfer satisfies the Stefan Boltzmann law:

$$W_c = h_c A_c (T_w - T_0) \quad (4)$$

$$W_r = 5.67 \varepsilon A_r \left[\left(\frac{273 + T_w}{100} \right)^4 - \left(\frac{273 + T_0}{100} \right)^4 \right] \quad (5)$$

where h_c is the coefficient of convective heat transfer, A_c – the area of convective heat transfer, ε – the blackness or emissivity of the object surface, which depends on the material and surface state of the object (such as roughness, oxidation degree, coating condition, etc.). In this paper, the blackness of the connector shell is 0.2, A_r – the radiant heat transfer area, and here is the surface area of the connector housing, which is equal to A_c .

According to the principle of thermoelectric equivalence, the thermal resistance is obtained by dividing the temperature rise by the thermal power. The diffusion thermal resistance of insulator $R_{\lambda 1}$ and the diffusion thermal resistance of shell $R_{\lambda 2}$ in fig. 3 are shown, respectively:

$$R_{\lambda 1} = \frac{T_c - T_j}{W_j} = \frac{\ln \frac{d_{jw}}{d_{jn}}}{2\pi\lambda_j l_j} \quad (6)$$

$$R_{\lambda 2} = \frac{T_j - T_w}{W_w} = \frac{\ln \frac{d_{ww}}{d_{wn}}}{2\pi\lambda_w l_w} \quad (7)$$

The convective thermal resistance, R_c , and radiation thermal resistance, R_r , of the connector shell are shown respectively:

$$R_c = \frac{T_w - T_0}{W_c} = \frac{1}{h_c A_c} \quad (8)$$

$$R_R = \frac{T_w - T_0}{W_r} = \frac{1}{5.67 \cdot 10^{-8} \varepsilon A_r (273 + T_w + 273 + T_0) [(273 + T_w)^2 + (273 + T_0)^2]} \quad (9)$$

Substituting the parameters in tab. 1 into the aforementioned equations, $R_{\lambda 1} = 9.125 \Omega$, $R_{\lambda 2} = 2.76 \text{ m}\Omega$, $R_C = 274.54/h_c \Omega$, and $R_R = 1097.62 \Omega$ can be calculated:

$$0.85 = \frac{T_c - T_w}{9.128} = \frac{T_w - 25}{\frac{274.54}{h_c} // 1097.62} = \frac{T_w - 25}{\frac{3.05 \cdot 10^5}{1097.62 h_c + 277.78}} \quad (10)$$

In order to calculate the contact conductor temperature, T_c , and the shell temperature, T_w , of the connector, the convective heat transfer coefficient, h_c , of the shell must be calculated first.

Calculation of the natural convective heat transfer coefficient

When the temperature rise is higher than 40 °C and the heat flux density is less than 0.04 [Wcm⁻²], natural-convection cooling can be selected to reduce the shell temperature of the connector. The heat transfer of natural air cooling depends on heat transfer coefficient and heat exchange area. The natural-convection heat transfer coefficient of air is generally between 5~25 W/m²°C, and can be assumed to be 10 W/m²°C in calculation. The h_c can also be estimated:

$$h_c = 2.5 \times \text{Posture coefficient} \times \left(\frac{\text{Temperature difference, } \Delta T}{\text{Feature size, } D} \right)^{0.25} \quad (11)$$

For the connector studied, the posture coefficient is 0.56, the temperature difference is 45 °C, the characteristic size is the shell length of 0.058 m, and the calculated $h_c = 7.4 \text{ W/m}^2\text{°C}$. It can be seen that the h_c values obtained by different methods are quite different. Because h_c value has great influence on the results of thermal simulation, based on Newton's cooling equation, the dimensional analysis method is used to calculate the heat transfer coefficient h_c of natural air-flow:

$$h_c = \frac{\text{Nu} \lambda_f}{D} = \frac{\lambda_f C (\text{Gr Pr})_m^n}{D} \quad (12)$$

where Nu is the dimensionless Nusselt number, Gr – the dimensionless Grashov number, Pr – the dimensionless Prandtl number, D – the characteristic dimension, coefficient C and index n are selected in tab. 2. The angle mark, m , indicates that the qualitative temperature, T , is the average value of solid surface temperature, T_w , and air temperature, T_0 , that is, $T = (T_w + T_0)/2$. The λ_f is the thermal conductivity of air, which can be found in tab. 3.

Table 2. The C and n values in the eq. (12)

	Gr × Pr value	Flow pattern	C	n	Feature size
Vertical plate and vertical cylinder	10 ⁴ -10 ⁹	Laminar flow	0.59	1/4	Height
	10 ⁹ -10 ¹³	Turbulent flow	0.10	1/3	
Horizontal cylinder	10 ⁴ -10 ⁹	Laminar flow	0.53	1/4	External diameter
	10 ⁹ -10 ¹²	Turbulent flow	0.13	1/3	
Horizontal plate with hot surface up	10 ⁶ -2 · 10 ⁷	Laminar flow	0.54	1/4	Square: side length, Disc: 0.9 × diameter, Sliver: short edge,
	2 · 10 ⁷ -3 · 10 ¹⁰	Turbulent flow	0.15	1/3	
Horizontal plate with hot surface downward	3 · 10 ⁶ -3 · 10 ¹⁰	Laminar flow	0.27	1/4	Rectangle: $L = 2ab/a + b$

Table 3. Physical parameters of dry air at one atmospheric pressure

T [°C]	ρ_v [kgm ⁻³]	C_p [Jkg ⁻¹ °C ⁻¹]	λ_f [Wm ⁻² °C ⁻¹]	$\alpha_v \cdot 10^{-2}$ [m ³ h ⁻¹]	$\mu \cdot 10^{-5}$ [kgm ⁻¹ s ⁻¹]	$\nu \cdot 10^{-5}$ [m ² s ⁻¹]	Pr
10	1.247	1005	2.51	7.22	1.80	14.16	0.705
20	1.205	1005	2.59	7.71	1.85	15.06	0.703
30	1.165	1005	2.67	8.23	1.90	16.00	0.701
40	1.128	1005	2.76	8.75	1.95	16.95	0.699
50	1.093	1005	2.83	9.26	2.00	17.95	0.698
60	1.060	1005	2.90	9.79	2.05	18.97	0.696
70	1.029	1009	2.97	10.28	2.10	20.02	0.694
80	1.000	1009	3.02	10.87	2.15	21.09	0.692

The Grashov number is the relationship between the buoyancy and viscosity of the fluid in the process of natural-convection, which is calculated in the eq. (13). The Prandtl number is the relationship between momentum diffusion and heat diffusion in the process of fluid-flow, which is calculated:

$$\text{Gr} = \frac{D^3 \alpha_v g \Delta T}{\nu^2} = \frac{D^3 \alpha_v g \rho^2 \Delta T}{\mu^2} \quad (13)$$

$$\text{Pr} = \frac{C_p \mu}{\lambda_f} \quad (14)$$

where ν is the kinematic viscosity of the air, μ – the dynamic viscosity of the air, α_v – the volume expansion coefficient of the air, ($=1/T$), T – the qualitative temperature, g – the acceleration of gravity, ρ_v – the density of the air, ΔT – the difference between the solid surface temperature, T_w , and the air temperature, T_0 , ($=T_w - T_0$), and C_p – the specific heat capacity of the air.

The calculation process of the natural convective heat transfer coefficient, h_c , is:

Determine the feature dimension, D , with the object posture. In this paper, the connector is placed horizontally, therefore, the characteristic dimension $D = d_{ww} = 20$ mm.

Calculate the qualitative temperature $T = (T_w + T_0)/2$. The ambient temperature $T_0 = 25$ °C, while the shell temperature, T_w , of the connector is not known. Therefore, temperature rise ΔT is assumed first, then T_w and T can be determined.

Calculate the volume expansion coefficient of air $\alpha_v = 1/T$, and get the physical parameters ν , λ_f , and Pr of air from tab. 3, and calculate the Gr.

Calculate the product of Gr and Pr, and determine the gas-flow state, coefficient, C , and index, n , from tab. 2.

Calculate the natural convective heat transfer coefficient, h_c , from eq. (12).

Calculate the temperature rise $\Delta T'$ from eq. (10).

Calculate the difference, δ , between the assumed temperature rise, ΔT , and the calculated temperature, $\Delta T'$, that is, $\delta = |\Delta T - \Delta T'|$. If $\delta > 0.5$ °C, the $\Delta T'$ will replace ΔT and return to Step 2 for a new round of iterative calculation. If $\delta < 0.5$ °C, the calculation process is completed, then h_c and T_w can be obtained.

The iterative calculation process of the coefficient h_c of the connector shell is:

- *The first iteration calculation:* assuming $\Delta T_1 = 15$ °C, because the ambient temperature $T_0 = 25$ °C, the surface temperature of the shell $T_{w1} = T_0 + \Delta T_1 = 40$ °C, and the qualitative temperature $T_1 = (T_{w1} + T_0)/2 = 32.5$ °C. According to tab. 3, the physical parameters of air at

32.5 °C are as follows, $Pr = 0.701$, $\nu = 16 \cdot 10^{-6} \text{ m}^2/\text{s}$, $\lambda_f = 2.67 \cdot 10^{-2} \text{ W/m}^\circ\text{C}$. Then, according to eqs. (13) and (14), the product of Grashov and Prandtl numbers can be calculated as 22125.6, larger than 10000.

It can be seen from tab. 2 that the air is laminar flow with coefficient $C = 0.53$ and index $n = 0.25$, then the coefficient $h_{c1} = 12.55 \text{ W/m}^2\text{C}$ can be calculated from eq. (12). Substituting it into eq. (10), $\Delta T_1' = T_w - T_0 = 16.8 \text{ }^\circ\text{C}$. Then the difference $\delta_1 = |\Delta T_1 - \Delta T_1'| = 1.8 \text{ }^\circ\text{C} > 0.5 \text{ }^\circ\text{C}$, so the second iteration is needed.

– *The second iteration calculation:* assuming $\Delta T_2 = \Delta T_1' = 16.8 \text{ }^\circ\text{C}$, then $T_{w2} = T_0 + \Delta T_2 = 41.8 \text{ }^\circ\text{C}$, $T_2 = (T_{w2} + T_0)/2 = 33.4 \text{ }^\circ\text{C}$. According to tab. 3, the physical parameters of air at 33.4 °C are as follows, $Pr = 0.701$, $\nu = 16 \cdot 10^{-6} \text{ m}^2/\text{s}$, $\lambda_f = 2.67 \cdot 10^{-2} \text{ W/m}^\circ\text{C}$, and the product of Grashov and Prandtl numbers can be calculated as 17983.4, larger than 10000.

It can be seen from tab. 2 that the air is laminar flow with coefficient $C = 0.53$ and index $n = 0.25$, then the convection heat transfer coefficient $h_{c1} = 12.8 \text{ W/m}^2\text{C}^{-1}$ can be calculated from eq. (12), which can be substituted into eq. (10) to calculate $\Delta T_2' = T_{w2} - T_0 = 16.45 \text{ }^\circ\text{C}$. Then $\delta_2 = |\Delta T_2 - \Delta T_2'| = 16.8 - 16.45 = 0.35 \text{ }^\circ\text{C} < 0.5 \text{ }^\circ\text{C}$, so the iterative calculation process is completed. Therefore, the convective heat transfer coefficient hc is $12.8 \text{ W/m}^2\text{C}$, the surface temperature of the shell is $41.5 \text{ }^\circ\text{C}$, and the surface temperature of the conductor is $50.7 \text{ }^\circ\text{C}$.

It should be noted that:

- The natural convective heat transfer coefficient calculated by the dimensional analysis method is more accurate than the other two methods.
- If the Rayleigh number $Ra = Gr \cdot Pr$ is less than the corresponding minimum value in tab. 2, the natural air cooling heat transfer can be ignored and only the heat conduction can be considered.
- The dimensional analysis method usually needs many iterations to make the error between the assumed temperature rise and the actual temperature rise less than $0.5 \text{ }^\circ\text{C}$. The calculation is cumbersome, which can be solved by programming with the help of calculation software such as MATLAB.

The ANSYS simulation analysis

Simulation results

The thermal performance of the connector is simulated by the electrothermal coupling module of ANSYS Workbench software. The connector model is shown in fig. 2, and the structure size and material parameters are defined according to tab. 1. The ambient temperature is $25 \text{ }^\circ\text{C}$, and the current load of 250 A is added at one end of the conductor, and the voltage load is 0 mV at the other end. The natural convective heat transfer coefficient of the shell shall be 12.8 W/m^2 , and the blackness shall be 0.2. The steady-state thermal simulation of the connector is carried out by automatic meshing method, and the temperature distribution nephogram is shown in fig. 4.

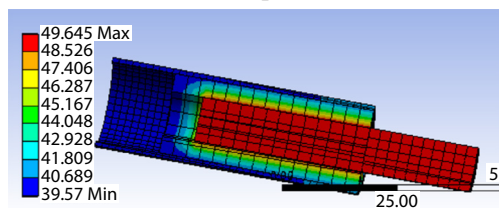


Figure 4. Temperature distribution of the connector section at 250 A current

The temperature results of each part of the connector are shown in tab. 4. The temperature rise of each part is less than $45 \text{ }^\circ\text{C}$, which meets the requirements of thermal performance. The relative error of thermal simulation is less than 6%, and the accuracy is high. Thermal simulation technology can get the temperature distribution, but the theoretical calculation and test can only get the temperature value of a single point. The temperature of the insulator

changes the most, therefore, in order to transfer the heat produced by the conductor quickly, the insulator material with high thermal conductivity should be selected.

Table 4. Temperature at each part of the connector [°C]

Name	Simulation results		Theoretical calculation results	Absolute error	Relative error [%]	Temperature rise
	Scope	Average				
Shell	39.6-41.9	40.8	43.4	-2.6	6.0	15.8
Insulator	41.9-48.5	45.2	43.4	1.8	4.1	20.2
Conductor	48.5-49.6	49.0	51.2	-2.2	4.3	24

Influencing factors

Insulator length

The insulator length [mm] of the connector is taken as 30, 35, 40, 44, 47, 50, and 55, respectively, to carry out electrothermal simulation, and the results are listed in tab. 5. When the insulator length is less than 44 mm, the temperature rise between different parts decreases with the increase of the insulator length. When the insulator length is greater than 44 mm, it has little effect on the temperature rise. The conductor temperature is at least 23.9 °C higher than that of the shell. The best insulator length is 44 mm.

Table 5. Temperature rise between parts of the connector with different insulator lengths

Insulator lengths [mm]	30	35	40	44	47	50	55
$T_w - T_0$ [°C]	13.1	11.2	10.1	10.1	9.9	9.9	9.8
$T_c - T_w$ [°C]	26.7	25.1	24.1	24.0	23.9	23.9	23.9
T_c [°C]	51.7	50.1	49.1	49.0	48.9	48.9	48.9

Shell length

The shell length [mm] of the connector is taken as 44, 48, 52, 58, 62, and 66, respectively, to conduct electrothermal simulation, and the results are shown in tab. 6. The temperature of conductor and shell decreases with the increase of shell length, and the decreasing rate is 1.3 and 1.5 °C/mm, respectively. The temperature rise between them increases slightly with the increase of shell length, and the increase value is less than 1 °C. When the shell length increases, the heat exchange area of natural air cooling increases, the heat exchange increases, and the temperature rise of connector decreases. The conductor temperature is at least 8.8 °C higher than that of the shell. Therefore, the shell length should be increased as much as possible.

Table 6. Temperature of each part of the connector with different shell length

Shell length [mm]	44	48	52	58	62	66
Shell temperature, T_w [°C]	44.9	43	41.5	39.6	38.5	37.5
Contact temperature, T_c [°C]	53.7	52.1	50.7	49	48.1	47.3
$T_c - T_w$ [°C]	8.8	9.1	9.2	9.4	9.6	9.8

Insulator material

When the insulator materials are PA66, PBT, and LCP, the electrothermal simulation of the connector is carried out, and the results are listed in tab. 7. When the insulator material is LCP, the conductor temperature, the shell temperature and the temperature difference are the lowest; when PBT is used, the conductor temperature and the shell temperature are the highest, and the temperature difference is in the middle; when the insulator material is PA66, the conductor temperature is in the middle, the shell temperature is the lowest, and the temperature difference is the maximum. Therefore, LCP with high thermal conductivity can be used as insulation material instead of PA66 to reduce the temperature of connector conductor and uniform temperature distribution of connector.

Table 7. Temperature of the connector with different insulator materials

Insulator material	Thermal conductivity λ_j [$\text{Wm}^{-1}\text{C}^{-1}$]	Conductor temperature T_c [$^{\circ}\text{C}$]	Shell temperature T_w [$^{\circ}\text{C}$]	$T_c - T_w$ [$^{\circ}\text{C}$]
PA66	0.33	48.7	39.6	9.1
PBT	0.27	49.7	40.9	8.8
LCP	0.57	44.0	39.6	4.4

Shell material

When the shell materials are zinc alloy, aluminum alloy and stainless steel, the electrothermal simulation of the connector is carried out, and the results are listed in tab. 8. When the shell material is aluminum alloy, the conductor temperature is the lowest, the shell temperature is in the middle, and the temperature difference between them is the smallest. When the shell is made of stainless steel, the conductor temperature is the highest, the shell temperature is the lowest, and the temperature difference is the largest. When the zinc alloy is used, the conductor temperature, the shell temperature and their temperature difference are all in the middle. Therefore, aluminum alloy with high thermal conductivity and blackness can be selected as the shell material to reduce the conductor temperature and uniform temperature distribution of connector.

Table 8. Temperature of the connector with different shell materials

Shell material	Thermal conductivity, λ_w [$\text{Wm}^{-1}\text{C}^{-1}$]	Blackness (Radiation coefficient)	Conductor temperature, T_c [$^{\circ}\text{C}$]	Shell temperature, T_w [$^{\circ}\text{C}$]	$T_c - T_w$ [$^{\circ}\text{C}$]
Zinc alloy	104.7	0.2	49.6	39.6	10.0
Aluminum alloy	234	0.55	48.5	39.0	8.5
Stainless steel	16	0.16	52.3	38.5	13.8

Conclusions

In this paper, the thermal performance of an electric vehicle charging connector is simulated and analyzed, and the following conclusions are obtained.

When the current flows through the contact conductor, Joule heat is generated due to the effect of the body resistance and the contact resistance of the conductor. The heat is transferred from the contact conductor through the insulator to the shell in the way of heat conduction, and then transferred to the atmospheric environment by natural-convection and radiation

mode. The thermal resistance of insulator and shell is in series, while that of convection and radiation is parallel.

The natural-convection heat transfer coefficient of the connector obtained by dimensional analysis and iterative calculation method is $12.8 \text{ W/m}^2\text{°C}$, which is more accurate than empirical value and empirical formula estimation, which provides accurate input parameters for thermal simulation calculation. When the working current of 250 A is applied and the ambient temperature is 25 °C , the temperature rise of the connector shell and conductor are 16.5 °C and 25.7 °C , respectively, meeting the temperature rise requirements of the connector.

In order to reduce the conductor temperature and uniform temperature distribution of connector, the following optimization schemes are proposed: The optimum length of the insulator is 44 mm. If the conditions permit, the shell length can be increased as much as possible. LCP with high thermal conductivity can be selected as the insulator material. The aluminum alloy with high thermal conductivity and blackness is selected as shell material.

Nomenclature

A_c, A_r – area of convective heat transfer and radiant heat transfer, respectively, [m^2]	R_R – thermal resistance through the radiation heat transfer, [°C/W]
C – coefficient, [–]	T_c, T_j, T_w, T_0 – temperature of conductor, shell, insulator and the external environment, respectively, [°C]
D – characteristic dimension, [m]	T – qualitative temperature, [°C]
d_{jw}, d_{in} – outer diameter and inner diameter of insulator, respectively, [m]	ΔT – difference between the solid surface temperature T_w and the fluid temperature T_0 , [°C]
d_{ww}, d_{wn} – outer diameter and inner diameter of shell, respectively, [m]	W_0 – thermal power generated by the connector, [W]
F – contact force between the pin and the crown spring socket, [N]	W_j, W_w – thermal power transmitted by heat conduction of insulator and shell cylinder wall, respectively, [W]
Gr – Grashov number, [–]	W_c, W_r – thermal power of convective and radiation heat transfer, respectively, [W]
g – acceleration of gravity, [m^2s^{-1}]	<i>Greek symbols</i>
l_d, d_d, H – resistivity [Ωm], length [m], diameter [m], and hardness [Nm^{-2}] of the contact conductor, respectively	α_v – volume expansion coefficient of the fluid, [m^3h^{-1}]
h_c – coefficient of convective heat transfer, [$\text{Wm}^{-2}\text{°C}^{-1}$]	μ – Dynamic viscosity of the fluid, [$\text{kgm}^{-1}\text{s}^{-1}$]
I – current, [A]	ν – kinematic viscosity of the fluid, [m^2s^{-1}]
l_j, l_w – length of insulator and shell, respectively, [m]	ε – Blackness or emissivity of the object surface, [–]
n – index, [–]	ζ – Deformation coefficient of the contact pin and the crown spring socket, generally $\zeta = 0.7$, [–]
Nu – Nusselt number, [–]	λ_j, λ_w – thermal conductivity of insulator and shell material, respectively, [$\text{Wm}^{-1}\text{°C}^{-1}$]
Pr – Prandtl number, [–]	ρ_v – density of the fluid, [kgm^{-3}]
R_b – resistance of the contact conductor, [Ω]	ρ – resistivity of the contact conductor, [Ωm]
R_j – contact resistance produced when the contact pin and the crown spring socket are contacted, [Ω]	
R_{i1}, R_{i2} – thermal resistance of insulator, shell, respectively [°C/W]	
R_c – thermal resistance of the natural-convection heat transfer of the air, [°C/W]	

Reference

- [1] Garrett, J. M., *et al.*, Thermal Management of Vehicle Cabins, External Surface, and Electronics: An Overview, *Engineering*, 5 (2019), 05, pp. 306-340
- [2] Chen, L. H., *et al.*, Thermal Design of Electric Cabinet for igh-resolution space camera, *Optics and Precision Engineering*, 19 (2011), 01, pp. 69-76

- [3] Liu, H., *et al.*, Application of Doped Gallium Based Liquid Metal Silicone Grease in Heat Dissipation of Electronic Devices, *Rare Metal Materials and Engineering*, 47 (2018), 09, pp. 2668-2674
- [4] Jiang, F., *et al.*, Thermal Design of Space Camera Baffle with Low Power, *Infrared and Laser Engineering*, 45 (2016), 09, pp. 189-194
- [5] Jiang, F., *et al.*, Thermal Design of Star Sensor Assembly, *Infrared and Laser Engineering*, 43 (2014), 11, pp. 3740-3745
- [6] Tang, Y., *et al.*, Development Status and Perspective Trend of Ultra-Thin Micro Heat Pipe, *Journal of Mechanical Engineering*, 53 (2017), 20, pp. 131-144
- [7] Su, X. H., *et al.*, Transient Thermal Analysis of a Plate Fin Heat Sink with Green's Function, *Chinese Journal of Aeronautics*, 24 (2011), 03, pp. 243-248
- [8] Wu, B., *et al.*, Numerical Investigation of Phase Change Thermal Control Unit for Portable Electronic Devices, *Journal of Beijing University of Aeronautics and Astronautics*, 36 (2010), 11, pp. 1330-1334
- [9] Nie, Y., *et al.*, Simulation Analysis and Test on Thermal Performances of Stratospheric Motor Controller, *Journal of Aerospace Power*, 33 (2018), 07, pp. 1758-1766
- [10] Ding, J., *et al.*, Thermal Analysis of IGBT Water-Cooling Radiator for Electric Vehicle Converter, *Journal of Central South University*, 48 (2017), 02, pp. 525-532
- [11] Wang, J. P., *et al.*, Simulation Analysis of Heat Transfer in the Hydraulic System of Loader, *Journal of Jilin University*, 46 (2016), 01, pp. 153-158